01 Oct 2022

Additive Manufacturing of Complexly Shaped SiC with High Density Via Extrusion-Based Technique – Effects of Slurry Thixotropic Behavior and 3D Printing Parameters

Ruoyu Chen

Adam Bratten

Joshua Rittenhouse

Tian Huang

et. al. For a complete list of authors, see https://scholarsmine.mst.edu/mec_aereng_facwork/4926

Recommended Citation

R. Chen et al., "Additive Manufacturing of Complexly Shaped SiC with High Density Via Extrusion-Based Technique – Effects of Slurry Thixotropic Behavior and 3D Printing Parameters," *Ceramics International*, vol. 48, no. 19, pp. 28444 - 28454, Elsevier, Oct 2022.
The definitive version is available at https://doi.org/10.1016/j.ceramint.2022.06.158

Ceramics International 48 (2022) 28444–28454

Contents lists available at ScienceDirect

Ceramics International

journal homepage: www.elsevier.com/locate/ceramint

Additive manufacturing of complexly shaped SiC with high density via extrusion-based technique – Effects of slurry thixotropic behavior and 3D printing parameters

Ruoyu Chen [a,b], Adam Bratten [b], Joshua Rittenhouse [b], Tian Huang [c], Wenbao Jia [c], Ming C. Leu [d], Haiming Wen [b,e,*]

[a] School of Metallurgical Engineering, Anhui University of Technology, Ma'anshan, Anhui, 243099, China
[b] Department of Materials Science and Engineering, Missouri University of Science and Technology, Rolla, MO, 65409, USA
[c] Department of Materials Science and Technology, Nanjing University of Aeronautics and Astronautics, Nanjing, Jiangsu, 210016, China
[d] Department of Mechanical and Aerospace Engineering, Missouri University of Science and Technology, Rolla, MO, 65409, USA
[e] Department of Nuclear Engineering and Radiation Science, Missouri University of Science and Technology, Rolla, MO, 65409, USA

ARTICLE INFO

Keywords:
Additive manufacturing
Silicon carbide
Rheological behavior
Printing parameters
Machine learning

ABSTRACT

Additive manufacturing of dense SiC parts was achieved via an extrusion-based process followed by electrical-field assisted pressure-less sintering. The aim of this research was to study the effect of the rheological behavior of SiC slurry on the printing process and quality, as well as the influence of 3D printing parameters on the dimensions of the extruded filament, which are directly related to the printing precision and quality. Different solid contents and dispersant- Darvan 821A concentrations were studied to optimize the viscosity, thixotropy and sedimentation rate of the slurry. The optimal slurry was composed of 77.5 wt% SiC, Y_2O_3 and Al_2O_3 powders, 0.25 wt% dispersant and 0.01 wt% defoamer. The printing parameters studied included extrusion pressure, nozzle size, layer height and printing speed; the one that had the most prominent effect on filament width and height was indicated as layer height. The nozzle inner diameter of 1.04 mm, speed of 350 mm/min, layer height of 0.7 mm and extrusion air pressure of 0.31 MPa were the optimal printing parameters. Furthermore, the relationship between the printing parameters and the filament dimensions was successfully predicted by using machine learning and grey system theory. Finally, the relative density of the printed SiC parts sintered at 1900 ^{o}C reached 94.7±1.5%.

1. Introduction

In recent years, SiC ceramic has become popular in many industries because of its excellent thermal conductivity, high-temperature strength and chemical stability [1–6]. Traditional methods for preparing dense SiC ceramic include casting and hot pressing [7,8]. However, these SiC ceramic forming techniques are limited in terms of low geometric accuracy, mold compatibility and long sintering time. In the recent years, electric-field assisted sintering of SiC ceramics is under considerable attention. Because it can significantly reduce the sintering temperature and time in structural ceramic materials [9]. Moreover, it is necessary to develop fabrication techniques to manufacture complexly shaped SiC ceramic.

Additive manufacturing (AM) is a rapidly evolving technology and is one approach toward fabricating SiC ceramic parts with complex geometries [10]. With the rapid development of science and technology, several AM techniques have been developed, such as extrusion [11], selective laser sintering [12], digital light processing [13] and direct ink writing [14]. Among the above AM techniques, extrusion processes possess some outstanding advantages such as low cost, good environmental adaptability, and controllability [15]. Zhang et al. successfully prepared SiC ceramic parts with periodic structure and outstanding mechanical properties by using an extrusion-based additive manufacturing technique combined with a liquid silicon infiltration process [16].

The key considerations for extrusion-based additive manufacturing processes are the preparation of slurries with good rheological behavior and feasible printing parameters. It has been reported that the viscosity

* Corresponding author. Department of Materials Science and Engineering, Missouri University of Science and Technology, Rolla, MO, 65409, USA.
E-mail address: wenha@mst.edu (H. Wen).

https://doi.org/10.1016/j.ceramint.2022.06.158
Received 15 April 2022; Received in revised form 3 June 2022; Accepted 14 June 2022
Available online 17 June 2022
0272-8842/Published by Elsevier Ltd.

Table 1
The formulation ratios of the powder mixture (wt.%).

	SiC	Al_2O_3	Y_2O_3
Powder mixture	95	3	2

and viscoelasticity of printing slurries can be improved by optimizing the amount of binder and solid content [17,18]. For instance, Zahra et al. optimized the printability of slurry by adjusting the type and content of additives, and established a relationship between the slurry properties and shape of final specimens [19]. Tang et al. investigated the effect of printing parameters on the shape of specimens using an orthogonal experiment [20]. The results showed that the printing parameters influenced the forming process in the following order: solids loading > layer height > print speed > nozzle diameter. For the extrusion additive manufacturing process, the printing parameters had a complicated relationship with the shape of printed specimens, which was difficult to analyze because of uncertainty and insufficient information. Grey system theory was used to study complex, multivariable systems while incorporating the unknown factors and discerning the relationship between the known factors and the results [21]. Chen et al. used grey system theory to successfully analyze the correlation between fly ash particle size and properties of insulation materials prepared with fly ash, which was proved to be a reliable basis for future work [22].

For the investigation of rheological behavior of printing slurries, most researchers have focused on the viscosity, storage modulus and loss modulus. However, thixotropic behavior is also an important property for printing slurries. Thixotropy describes a reduction of the structural strength during a constant shear load phase and a complete regeneration of the structure during the subsequent rest phase [23]. In an extrusion-based AM process, this means that the printing slurry becomes more viscous when it is not actively being printed, which enables more precise stopping during printing. Moreover, very few researchers have investigated in detail the relationship between the printing parameters and shape of filament and used their findings to build a predictive model. To address these knowledge gaps, the viscosity and thixotropic behavior of SiC slurries in this study were optimized by adjusting the amount of dispersant and solid content. Furthermore, the influence of the printing parameters including pressure, layer height and nozzle speed on the width and height of filament was investigated by using grey system theory. A corresponding prediction model, which can be used to select printing parameters based on the required precision of extrusion, was successfully built by machine learning.

2. Materials and methods

2.1. Slurry preparation

The raw materials consisted of commercial SiC powder (purity ≥99%, average particle size 0.45 μm, Weifang Huarong Ceramic Company, China), α-Al_2O_3 powder (purity ≥99%, average particle size 0.8 μm, US Research Nanomaterials, USA) and Y_2O_3 powder (purity ≥99.9%, average particle size 0.95 μm, Atlantic Equipment Engineers, USA). Darvan 821A and ethanol were used as dispersant and defoaming agent, respectively.

The formulation ratios of the powder mixture for the slurries are represented in Table 1. Slurries with solid content ranging from 71.5 to 79 wt% were mixed by planetary ball milling. The ball-to-powder ratio, milling speed and milling time were 2:1, 350 RPM and 180 min, respectively. Finally, the pH value of the slurry was adjusted to 10 using sodium hydroxide solution in order to improve the stability of the suspension.

2.2. Additive manufacturing and subsequent processing and sintering

The SiC slurries were printed using a modified commercial 3D printer (Lulzbot TAZ 6) retrofitted with a compressed air module. The 3D models were built in Microsoft 3D builder and sliced using Simplify3D software, and then exported to G-code. A Python script developed in-house was used to modify the G-code to control the application of compressed air and syringe pathing. The modified code was then executed by Simplify3D. In order to determine the optimal parameters for printing specimens with complex geometries, the printing parameters of layer height, applied air pressure, nozzle speed and nozzle size were varied. After printing and subsequently drying at 110 °C for 24 h, the specimens were treated at 600 °C for 1 h to pyrolyze the dispersant. Finally, electric field-assisted liquid phase sintering was performed in a DCS-10 (Thermal Technologies, Inc.) under argon atmosphere using a graphite crucible designed to prevent pressure from being applied to the specimens. A powder bed containing SiC, Al_2O_3, and Y_2O_3 powders was utilized inside the crucible to inhibit volatilization at high temperature [24]. The heating schedule is presented in Fig. 1.

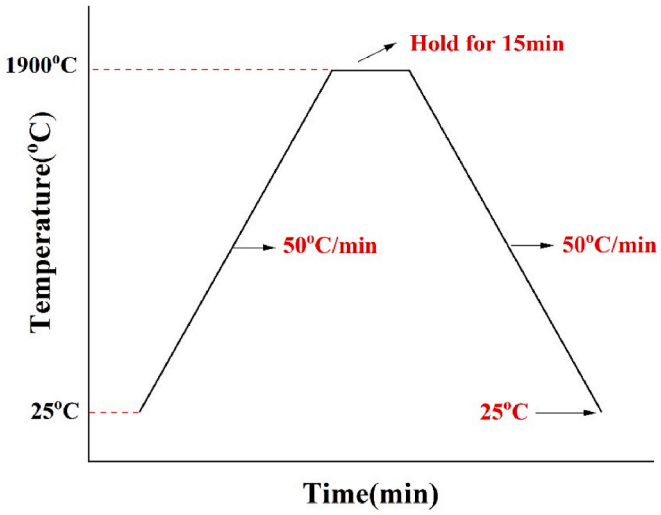

Fig. 1. Heating schedule for electric field-assisted liquid phase sintering.

2.3. Characterization

The rheological behavior of the slurries was measured using a

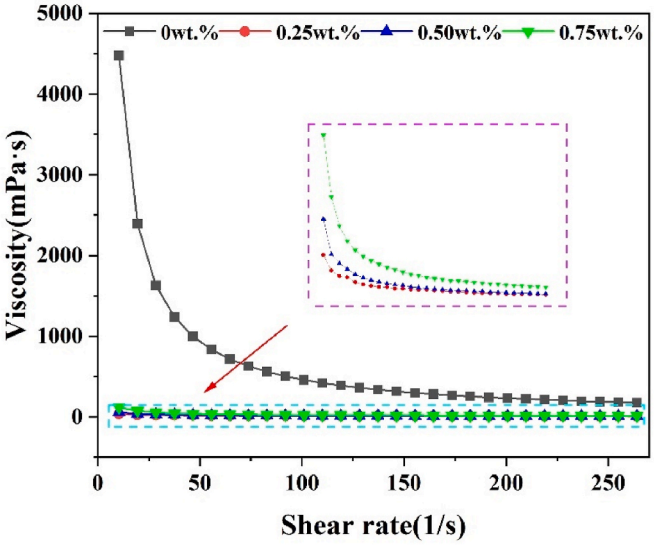

Fig. 2. Effect of dispersant concentration on the viscosity of the slurry with 71.5 wt% solid content.

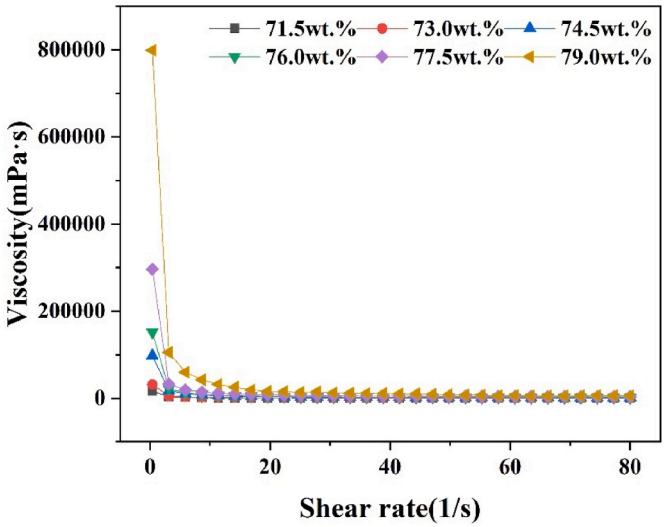

Fig. 3. Effect of solid content on the viscosity of the slurries.

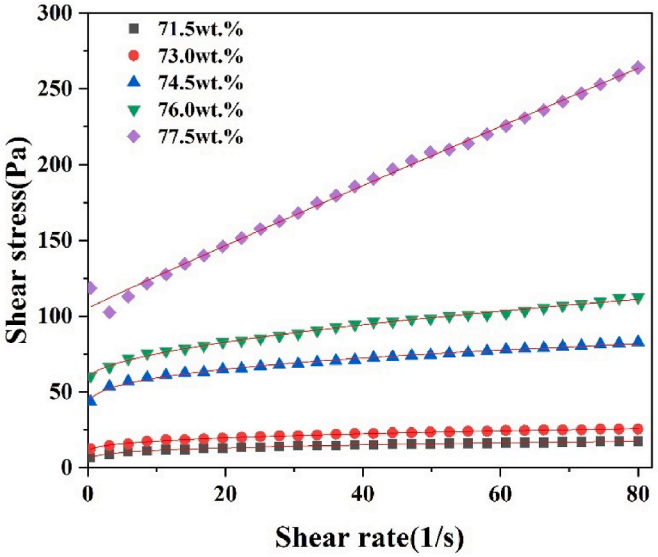

Fig. 4. The relationship between shear rate and shear stress for slurries with various solids loading.

viscometer (HBDB-II + PRO Brookfield); the viscosity and shear stress were measured under a continuous shear rate from 0.4 s^{-1} to 80 s^{-1} at room temperature. The surface of the green bodies was observed using an optical microscope. The density of the sintered SiC specimens was measured by Archimedes method. The microstructures of the sintered specimens were analyzed using scanning electron microscopy (FEI Quanta 600) in low-vacuum mode with ions ionizied from water vapor as the charge-reducing species.

3. Results and discussion

3.1. Rheological behavior of slurries

It was determined that the necessary condition for the preparation of dense specimens is a printing slurry with high solid content. However, the viscosity of the high solid-content slurry was too high to print specimens by extrusion. Therefore, optimization of the rheological behavior of slurries with high solid content is imperative to the success of the extrusion-based additive manufacturing process. Darvan 821A was used as dispersant to improve the flowability of slurry. The effect of dispersant concentration on the viscosity of slurry is displayed in Fig. 2. The viscosity of the slurry decreased with the initial addition of dispersant, as expected. The difference in the slurry viscosity among different dispersant contents was more pronounced at low shear rates. The main reason for this phenomenon is strong adsorption energy of the dispersant onto the ceramic powder. The dispersant easily covered the surfaces of the SiC, Al_2O_3 and Y_2O_3 powders, which improved the dispersion stability through steric hindrance and electrostatic stabilization [25]. However, when more dispersant was added to the slurry, the viscosity increased gradually. At high concentrations, excess dispersant could cause flocculation of slurry through a depletion mechanism [26]. Osmotic pressure was caused by steric hindrance because the distance between the powders was too short to hold the excess dispersant molecules. The generated osmotic pressure may have produced an attractive force between the ceramic powders, resulting in the flocculation of the SiC particles [27]. At the same time, the excess dispersant molecules were interconnected to form a network structure, leading to reduced flowability of the ceramic powders in the slurry [28].

Based on the experimental results shown in Fig. 2, the optimal concentration of dispersant was 0.25 wt%. With that, the effect of solid content on the flowability and thixotropic behavior of slurry was investigated. The viscosity of slurries with 71.5, 73, 74.5, 76, 77.5 and 79 wt% solids loading with 0.25 wt% dispersant at pH 10 is presented in Fig. 3. As the solid content increased, the slurry became more viscous.

Table 2
The rheological parameters and correlation coefficient for slurries with different solids loading.

Specimens	τ_0 (Pa)	κ (Pa·s)	n	R^2
77.5 wt% slurry	105.19	2.27	0.97	0.9936
76.0 wt % slurry	58.51	4.62	0.56	0.9955
74.5 wt% slurry	38.44	9.21	0.35	0.9952
73.0 wt% slurry	9.59	3.60	0.34	0.9948
71.5 wt % slurry	2.47	5.06	0.25	0.9952

Interestingly, it was observed that when the solid content of slurry increased from 77.5 wt% to 79 wt%, the viscosity increased sharply at low shear rates. According to the Woodcook model, the continuous phase in the slurry influences the slurry flowability (Equation (1)) [25]:

$$\frac{h}{d} = \left(\frac{1}{3\pi\Phi} + \frac{5}{6}\right)^{1/2} - 1 \tag{1}$$

where h represents the distance between SiC, Al_2O_3 and Y_2O_3 powders, d is the diameter of powder particles, and Φ corresponds to the volume of the solid loading of the slurry. It was found that with increasing content of the ceramic powders the average distance between the powders decreased. Meanwhile, the van der Waals forces increased significantly. Therefore, increasing the solid content of the slurry hindered the flow of the slurry, leading to an increase in slurry viscosity. The 79 wt% slurry was too viscous to extrude from the nozzle. As the shear rate increased, all of the slurries showed pseudoplastic (shear thinning) behavior (Fig. 4). The Herschel-Bulkley model is used to represent the pseudoplastic property of the slurry (Equation (2)) [26]:

$$\tau = \tau_0 + \kappa\gamma^n \tag{2}$$

where τ is shear stress, τ_0 is yield stress, γ is applied shear rate, κ is the consistency index, and n is the shear-thinning index. The experimental results are consistent with the Herschel-Bulkley model (Table 2). The shear-thinning indices of the slurries were lower than 1, which demonstrated that all of the slurries can be considered non-Newtonian fluids. Shear-thinning behavior of non-Newtonian fluids enabled the slurry to be extruded smoothly and to rapidly solidify in the absence of shear force after extrusion [29]. Therefore, all of the prepared slurries were suitable candidates for the printing slurry of the extrusion additive manufacturing process. Moreover, with the increase in the solid content

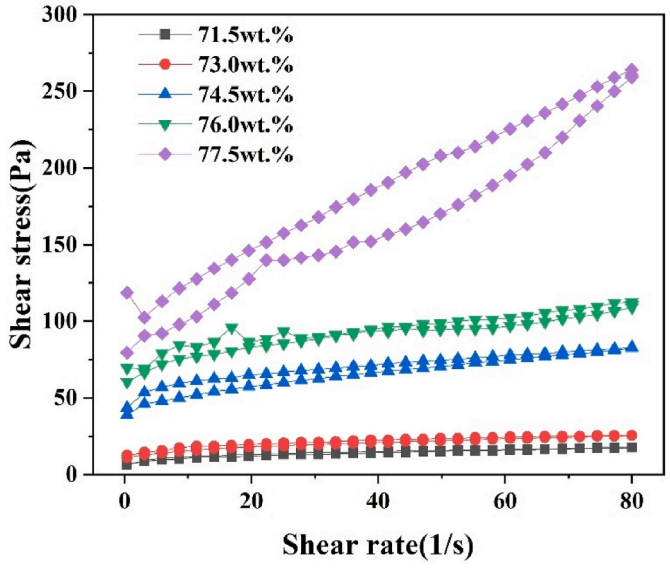

Fig. 5. Thixotropy loops of slurries with different solid contents.

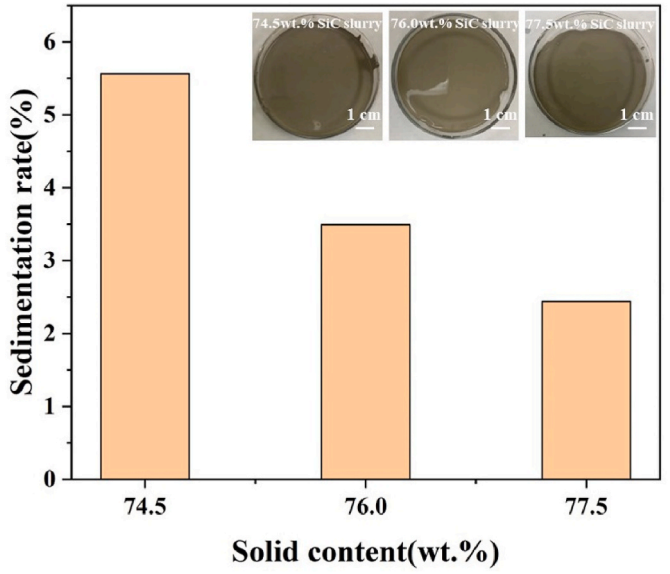

Fig. 6. Sedimentation rate of the slurries with 74.5, 76.0 and 77.5 wt% solid content.

of the slurry, the yield stress increased gradually. When the slurry solid content was lower than 74.5 wt%, the yield stress of the SiC slurry was lower than 10 Pa, which had a negative influence on the extrusion, since it is difficult to maintain during the printing process the structure of a paste with a lower yield stress.

Thixotropy is a time-dependent phenomenon, as the viscosity of the substance must recover after a certain period of time when the applied force is removed [30]. Thus, thixotropy of slurry plays an important role in printing specimens with complex geometries. Fig. 5 shows the thixotropy loops of slurries with different solid contents. Stronger thixotropic behavior is represented by a larger area between the top and bottom of the curve. The solid content of the slurry was found to have a great influence on the thixotropic behavior. The thixotropy of the slurry improved considerably when the slurry solid content increased. Thixotropy is caused by a competition between the ceramic powder interactions and viscous forces [31]. The distance between the ceramic powder particles in the slurry decreased with increasing solid content of the slurry, resulting in the improvement of interactions between ceramic particles. Compared to the slurries with 74.5, 76.0 and 77.5 wt% solid contents, the slurries with 71.5 wt% and 73.0 wt% exhibited poor thixotropy. Furthermore, when performing practical experiments, the slurries with 71.5 wt% and 73.0 wt% solids loading were not suitable for printing specimens because of their high flowability and low shape retention.

The solid content of the slurries was also found to affect the sedimentation rate (Fig. 6). The sedimentation rate decreased with increasing solid content, which was due to interactions between the SiC, Al_2O_3 and Y_2O_3 powders in the slurry. The stronger the interaction between ceramic powders, the lower the sedimentation rate.

When the slurry was used to print filament by the extrusion additive manufacturing process, occasionally some flaws like warpage occurred, which was due to the poor thixotropic behavior of slurry. Optical micrographs of the extruded filaments are shown in Fig. 7. Warpage flaws were observed in the filaments prepared with 74.5 and 76.0 wt% solid contents. While the track lines of the 77.5 wt% solids loading slurry appeared to be relatively straight and free of deformations, the track lines printed using slurries with lower solids loading tended to warp or bend during the drying process. During the extrusion process, the slurry was subjected to shear stress, which decreased the viscosity of the SiC slurry, resulting in the improvement of the slurry flowability. However, after extruding, the shear stress was removed and the viscosity of the slurry could not recover quickly enough due to the poor thixotropy of the slurry. Therefore, the extruded slurries still had good flowability and demonstrated the formation of warpage flaws during drying. For the specimens prepared with 77.5 wt% SiC slurry, few warpage flaws were formed in the specimens. This is presumably due to the high thixotropy of the slurry as shown in Fig. 5.

According to the Herschel-Bulkley model and Newton's law, the shear rate affects the shear stress and viscosity of slurry. For pseudoplastic fluids, with increasing shear rate, the shear stress and viscosity of slurry increase and decrease, respectively. During extrusion, the shear rates of the 77.5 wt% slurry extruded through different nozzle sizes were different. The shear rate γ of the slurry was calculated by Equation (3) [14]:

$$\gamma = \frac{4Q}{\pi(d/2)^3} \tag{3}$$

where Q represents the flow rate and d is the diameter of the nozzle. Table 3 shows the shear rates of the slurry with 77.5 wt% solid content using nozzles with different sizes during extrusion. When a 1.04 mm nozzle was utilized to extrude the SiC slurry with 77.5 wt% solid content, the shear rate reached maximum value (88.49 1/s). At the same time, the area of thixotropy loop was changed (Fig. 8). It was deduced that when a 1.04 mm nozzle was used to extrude the 77.5 wt% slurry, the recovery rate of the viscosity of the slurry was higher than others during the extrusion process. Therefore, the 1.04 mm nozzle was determined to be most suitable for printing high-quality specimens.

3.2. Prediction of filament dimensions by grey incidence analysis and machine learning

For the extrusion process, it is important to control the dimensions of the extruded filament, which affects the printing precision and quality. It was observed that when SiC pastes with low viscosity were used, the filament height was equal to the layer height because of their high flowability (Fig. 9). However, when SiC pastes with high viscosity and un-optimized printing parameters were used for printing, excess paste piled up on both sides of the nozzle, resulting in the formation of gaps between each layer of filament. Therefore, under this condition, the filament height was not equal to the layer height. The printing parameters such as pressure, layer height and nozzle speed have a great influence on the shape and dimensions of the extruded filament; however,

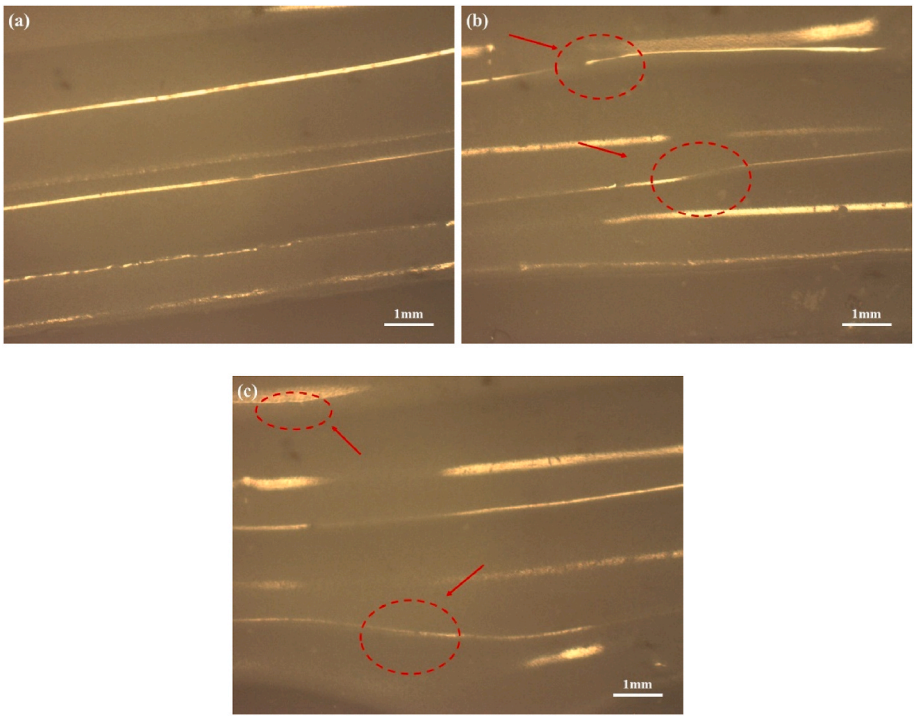

Fig. 7. Optical images of filaments extruded using the slurries analyzed in Fig. 6: (a) 77.5 wt% SiC slurry; (b) 76.0 wt% SiC slurry; (c) 74.5 wt% SiC slurry. Sites where track lines were significantly deformed are circled to call attention to warpage defects.

Table 3
Shear rates of the 77.5 wt% slurry during extrusion through nozzles with different diameters.

Nozzle diameter	0.60 mm	0.70 mm	1.04 mm	1.34 mm
Shear rate (1/s)	62.24	50.56	88.49	59.26

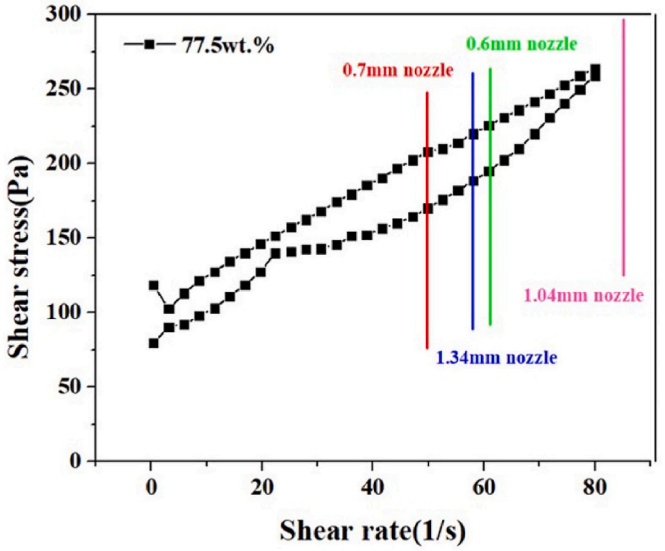

Fig. 8. Thixotropy loop of a slurry with 77.5 wt% solid content, with annotations added to reflect the shear rates experienced during extrusion through different nozzle diameters.

it is very time-consuming to find such relationship experimentally. Grey incidence analysis, an effective method to investigate the relationship between factors and results [32–34]. In this work, the printing parameters and the dimensions of extruded filament were regarded as input factors and output factors, respectively. The grey relational grade obtained from the grey incidence analysis was used to optimize the printing parameters and the accuracy of filament dimension prediction by machine learning. The results from studying the effects of printing parameters on the dimensions of the extruded filament are displayed in Appendix Fig. A1. Based on these results, the grey relational grades between printing parameters and the filament dimensions were calculated and are presented in Table 4.

It was found that layer height had the highest grey relational grade with both the width and height of the extruded filament. Therefore, the layer height had a more significant influence on the dimensions of the extruded filament compared with the other processing parameters. Therefore, future work on 3D printing with high viscosity slurry should pay specific attention to adjusting the printing parameters, especially layer height, to reduce the porosity in the matrix and optimize the dimensions of the printed filament. Moreover, among the printing parameters, the nozzle speed showed the lowest grey relational grade. These findings played a major role in building a prediction model using machine learning. Machine learning prediction models, specifically artificial neural network, trained using high quality databases have been shown to help identify the elementary semi-empirical rules that dictate the relationship between input factors and output factors and further predict the outcomes in the same system for input data that are not in the training database [35]. In this work, the printing parameters of pressure, layer height and nozzle speed were considered as input parameters, and the dimensions of extruded filament including height and width were regarded as output parameters. A database with 62 data sets was used for the prediction model. The accuracy of the model predictions was evaluated by using relative error (Equation (4)):

$$\delta = \left| \frac{(v_A - v_E)}{v_E} \right| \tag{4}$$

where δ is the relative error and v_A and v_E are actual value and predicted values, respectively. A schematic diagram for the building and optimizing processes of the prediction model can be found in Appendix

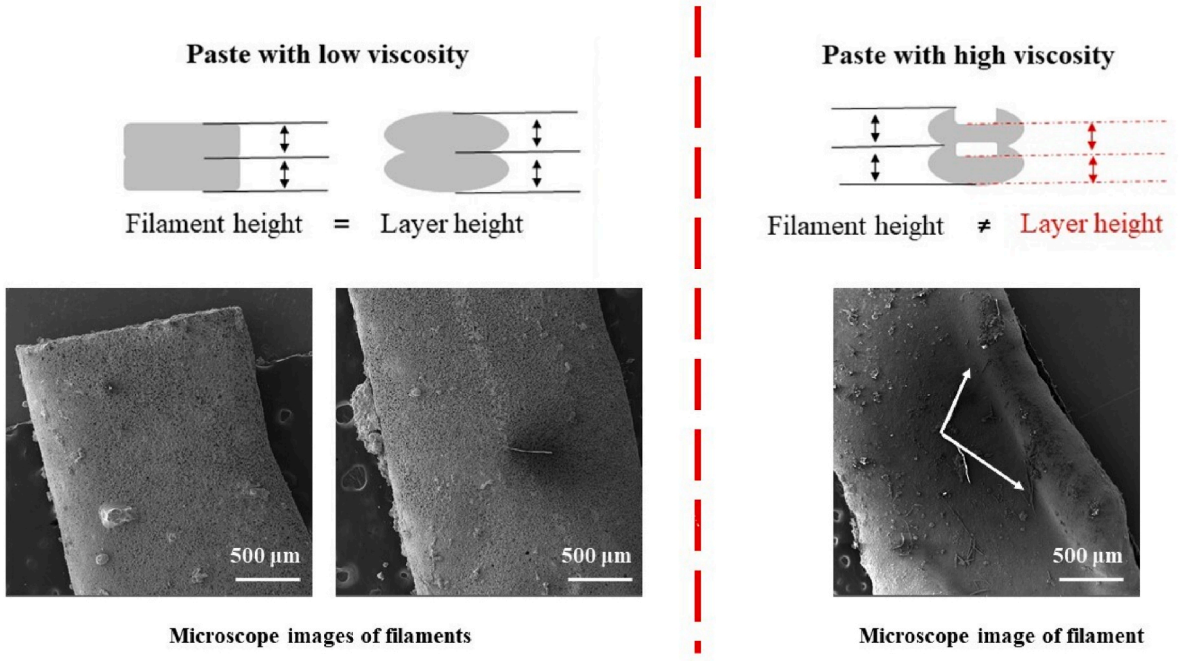

Fig. 9. Schematics of filament height versus layer height under different conditions and microscope images of filament prepared with different slurries.

Table 4
Grey relational grades between individual printing parameters and the dimension of the extruded filament. Higher values reflect a stronger dependence.

	Layer height	Nozzle speed	Pressure
Grey relational grade	0.9984	0.3336	0.8939

Fig. A2. The process included three layers: input layer (the printing parameters), hidden layer and output layer (the height and width of the filament). The hidden layer was used to find the relationship between input layer and output layer. Fig. 10 shows the predicted values of filament width and height from the artificial neural network model, along with actual data obtained from the experiments. The mean values of relative error of width and height (δ) were equal to 0.045 and 0.100, respectively, which indicated that the model effectively predicted the dimensions of extruded filament. Therefore, the model can be used to select printing parameters based on the intended degree of precision. Because different levels of precision may be required based on the application and the intended post-processing, the model is a powerful tool for selecting the best printing parameters without trial and error, saving time and resources for parts production.

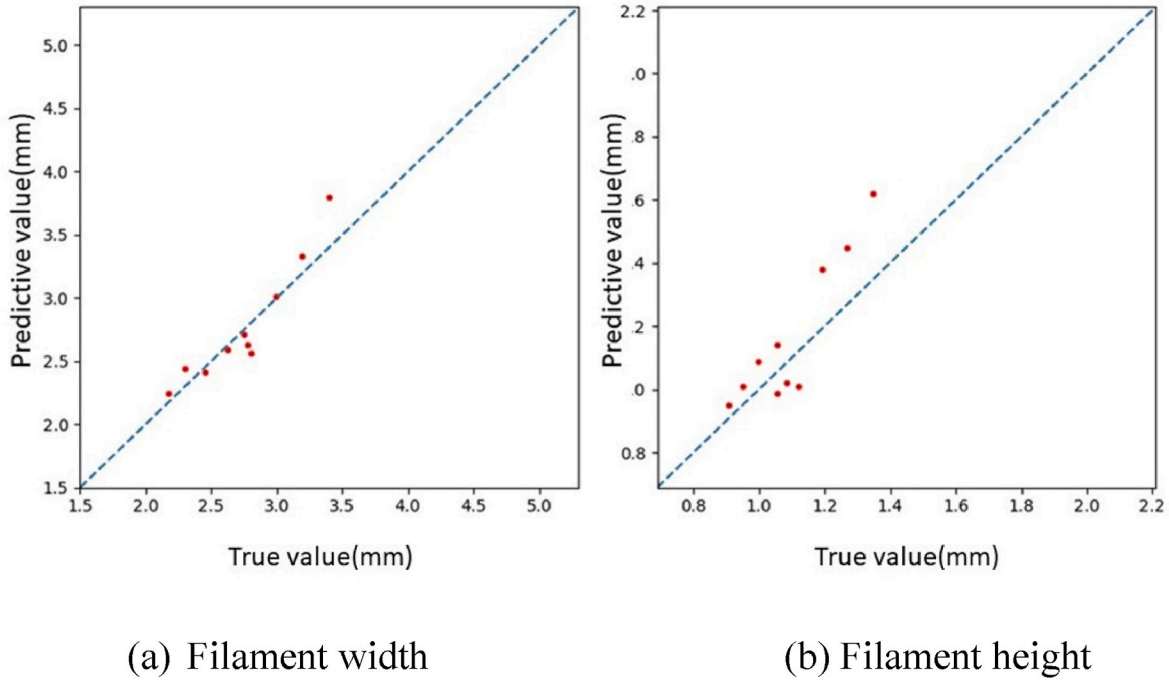

Fig. 10. The accuracy of the machine learning model for predicting filament dimensions.

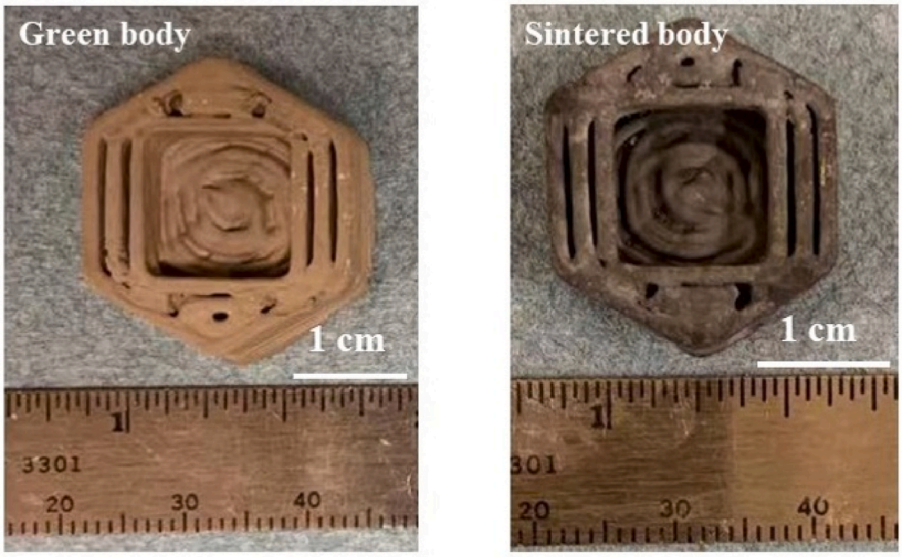

Fig. 11. Optical images of a printed part before and after sintering.

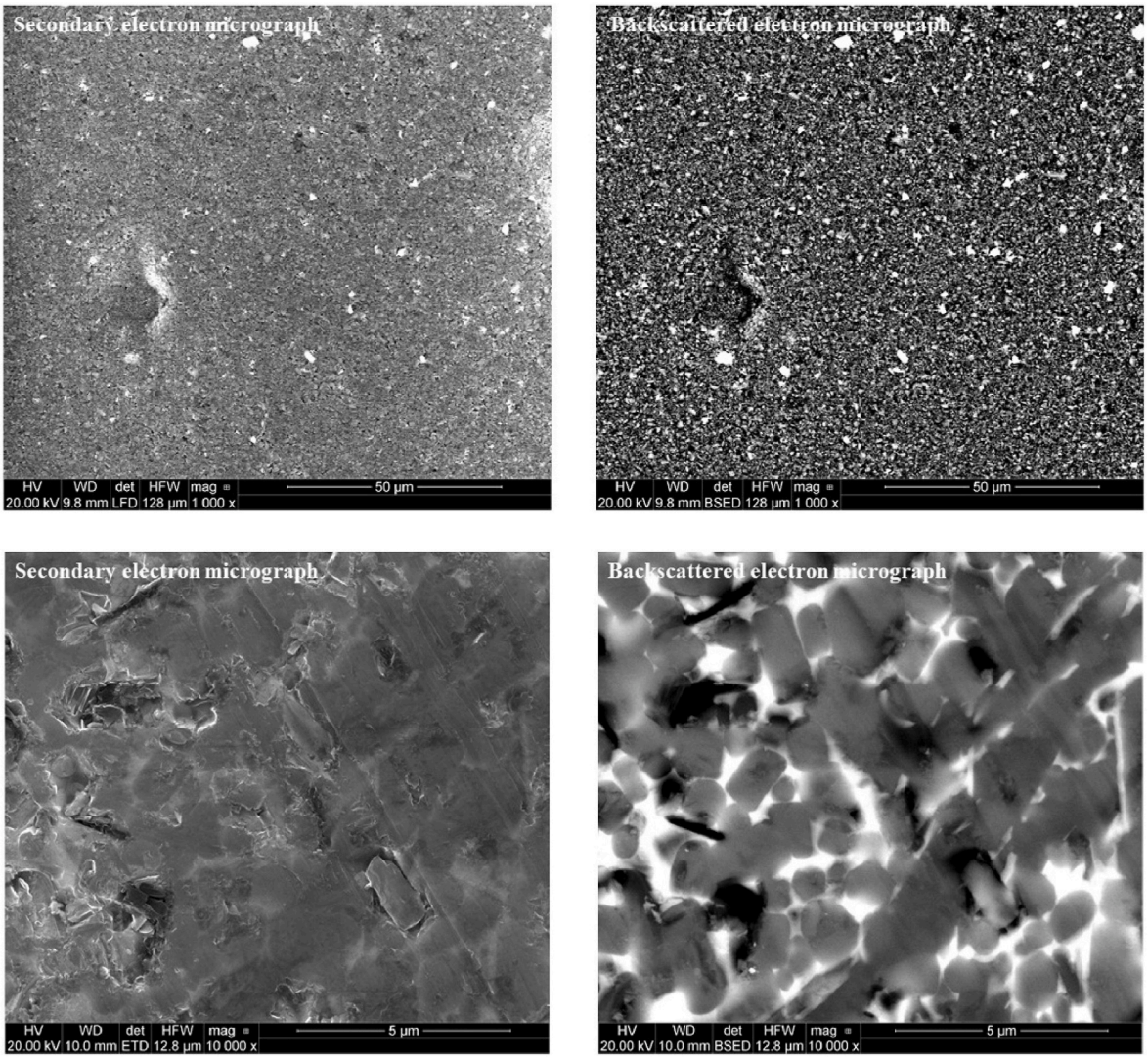

Fig. 12. Scanning electron micrographs of green (top) and electric-field assisted liquid-phase sintered (bottom) specimens. Secondary electron images are presented to highlight the morphology, while backscattered electron images illustrate the distribution of the oxide sintering aids before and after sintering.

3.3. Density and microstructure of sintered specimens

Based on the above results, when the pressure, nozzle speed and layer height were chosen to be 0.31 MPa, 300 mm/min and 0.65 mm, respectively, the filament with excellent shape was obtained. After field-assisted sintering, the shape of the SiC specimens did not change (Fig. 11). Furthermore, because of the high solid content of the printing slurries, little shrinkage (9.33 ± 0.8%) occurred along the height direction during sintering. Due to the high solid content and low shrinkage, highly dense SiC ceramic parts (bulk density ~3.08±0.05 g/cm^3, relative density ~94.7±1.5%) with complex geometries were obtained.

Fig. 12 presents the microstructure of green and sintered specimens. The green body is relatively dense with few pores because of the high solid content in the slurry. After sintering, highly dense specimens were obtained, owing to the formation of the liquid yttrium aluminate phase at high temperature and the presence of electrical field promoting pressure-less sintering. The liquid phase filled into the pores caused by the evaporation of water. As a direct consequence, the liquid phase improved the sintering ability of SiC powders [36]. Moreover, the powder bed used during sintering played a key role in inhibiting the volatilization of oxides, reducing the weight loss caused by the reactions between SiC and Al_2O_3 or Y_2O_3 (Equations (5) and (6)) [37]:

$$SiC_{(s)} + Al_2O_{3(s)} \rightarrow Al_2O_{(g)} + SiO_{(g)} + CO_{(g)} \quad (5)$$

$$SiC_{(s)} + Y_2O_{3(s)} \rightarrow Y_2O_{(g)} + SiO_{(g)} + CO_{(g)} \quad (6)$$

4. Conclusions

Dense SiC ceramic parts with complex geometries were prepared by an extrusion-based additive manufacturing process combined with field-assisted pressure-less sintering. Slurries were prepared with a range of solid contents to determine the optimum composition for printing. The slurry with 77.5 wt% solid content and 0.25 wt% dispersant showed excellent thixotropic behavior. The thixotropy of the slurry was found to have a great influence on the additive manufacturing process and the quality of extruded filament after drying. In addition, the relationship between printing parameters and extrusion quality/precision was investigated. The layer height was found to be particularly influential, having the highest relevance coefficient with the dimensions of the extruded filament based on grey relational grades obtained via grey incidence analysis. A model was established using machine learning for predicting the appropriate input parameters based on the desired print quality/precision. The model can be used to determine the necessary printing parameters for specimens requiring a specific amount of precision based on the intended application. Finally, the density of the sintered specimens with complex geometry reached 3.08±0.05 g/cm^3 (relative density ~94.7±1.5%).

Declaration of competing interest

The authors declare that they have no known competing financial interests or personal relationships that could have appeared to influence the work reported in this paper.

Acknowledgements

This study was supported by a seed grant from the Advanced Manufacturing Signature Area of Missouri University of Science and Technology. J. Rittenhouse thanks the Office of Nuclear Energy of U.S. Department of Energy for an Integrated University Program graduate fellowship. H.M. Wen also acknowledges the U.S. Nuclear Regulatory Commission Faculty Development Program (award number NRC 31310018M0044).

Appendix

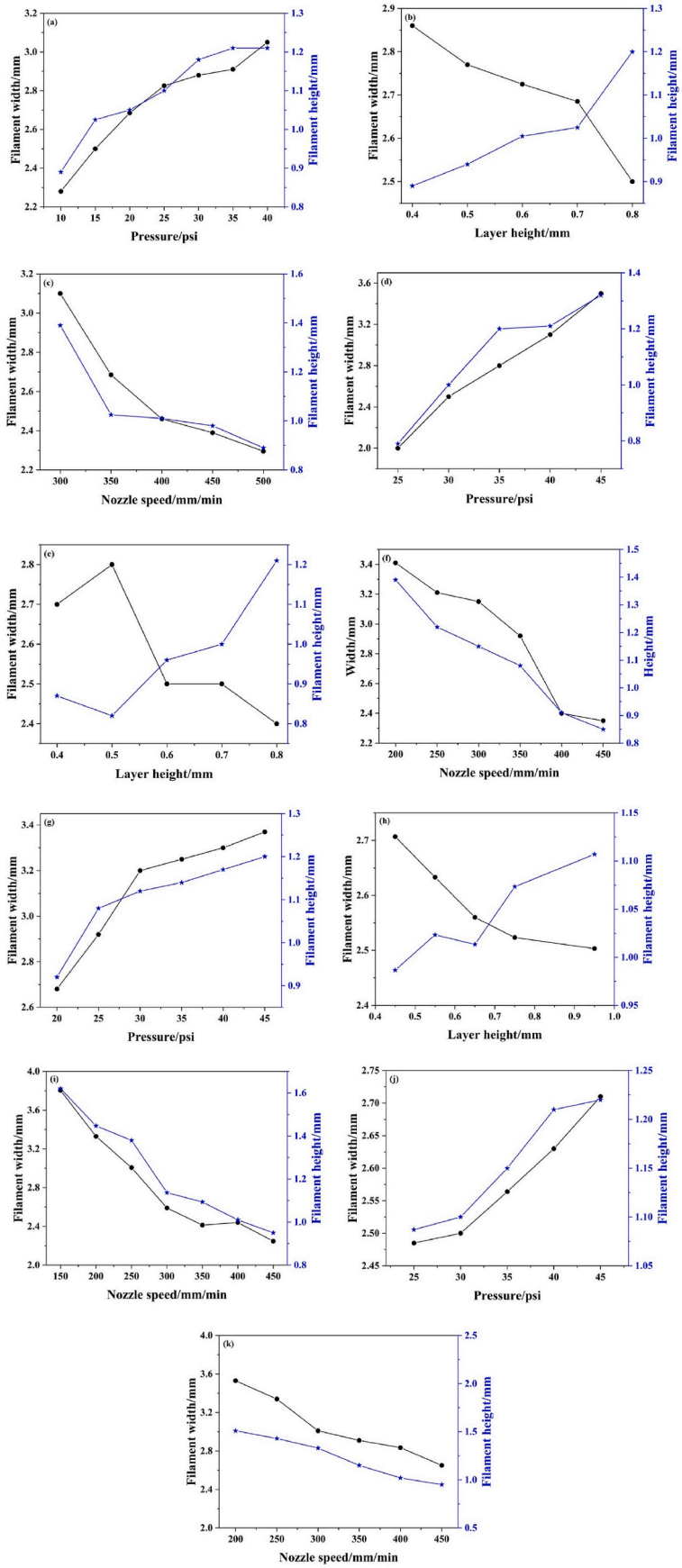

Fig. A1. Effects of printing parameters (pressure, layer height and nozzle speed) on the dimensions (width and height) of extruded filament. (a) Effects of pressure on filament width/height, with a layer height and a nozzle speed of 0.5 mm and 350 mm/s, respectively; (b) Effects of layer height on filament width/height, with a

pressure and a nozzle speed of 20 psi and 330 mm/s, respectively; (c) Effects of nozzle speed on filament width/height, with a layer height and pressure of 0.65 mm and 18 psi, respectively; (d) Effects of pressure on filament width/height, with a layer height and nozzle speed of 0.4 mm and 380 mm/s, respectively; (e) Effects of layer height on filament width/height, with a pressure and a nozzle speed of 18 psi and 370 mm/s, respectively; (f) Effects of nozzle speed on filament width and height, with a layer height and pressure of 0.5 mm and 21 psi, respectively; (g) Effects of pressure on filament width and height, with a layer height and a nozzle speed of 0.6 mm and 330 mm/s, respectively; (h) Effects of layer height on filament width/height, with a pressure and a nozzle speed of 23 psi and 410 mm/s, respectively; (i) Effects of nozzle speed on filament width/height, with a layer height and a pressure of 0.65 mm and 15 psi, respectively; (j) Effects of pressure on filament width/height, with a layer height and a nozzle speed of 0.75 mm and 450 mm/s, respectively; (k) Effects of nozzle speed on filament width/height, with a layer height and a pressure of 0.65 mm and 25 psi, respectively.

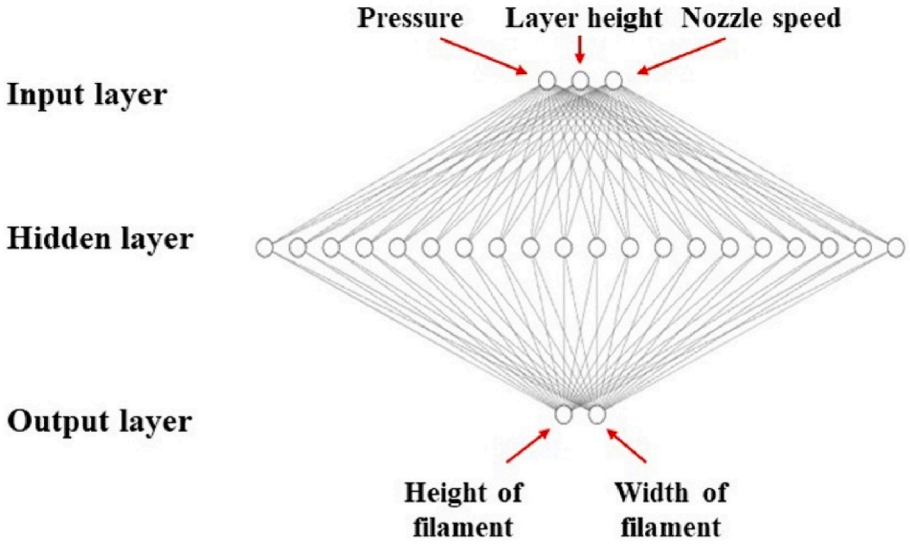

Fig. A2. Schematic for building and optimizing processes of the machine-learning prediction model.

References

[1] M. Li, X. Zhou, H. Yang, S. Du, Q. Huang, The critical issues of SiC materials for future nuclear systems, Scripta Mater. 143 (2018) 149–153, https://doi.org/10.1016/j.scriptamat.2017.03.001.

[2] Y. Katoh, A. Kohyama, T. Hinoki, L.L. Snead, Progress in SiC-based ceramic composites for fusion applications, Fusion Sci. Technol. 44 (2003) 155–162, https://doi.org/10.13182/FST03-A326.

[3] A.M. Parvanian, H.R. Salimijazi, M. Fathi, M. Saadatfar, Synthesis and thermal shock evaluation of porous SiC ceramic foams for solar thermal applications, J. Am. Ceram. Soc. 102 (2019) 2009–2020, https://doi.org/10.1111/jace.16007.

[4] H. Dong, Z. Fang, T. Yang, Y. Yu, D. Wang, K.C. Chou, X. Hou, Single crystalline 3C-SiC whiskers used for electrochemical detection of nitrite under neutral condition, Ionics 22 (2016) 1493–1500, https://doi.org/10.1007/s11581-016-1666-5.

[5] L. Zhou, T. Yang, L. Zhu, W. Li, S. Wang, X. Hou, X. Mao, Z. Wang, Piezoelectric nanogenerators with high performance against harsh conditions based on tunable N doped 4H-SiC nanowire arrays, Nano Energy 83 (2021), 105826, https://doi.org/10.1016/j.nanoen.2021.105826.

[6] L. Zhou, L. Zhou, T. Yang, X. Hou, Z. Du, S. Cao, H. Wang, K.C. Chou, Z.L. Wang, Ultra-stable and durable piezoelectric nanogenerator with all-weather service capability based on N doped 4H-SiC nanohole arrays, Nano-Micro Lett. 14 (2022) 1–10, https://doi.org/10.1007/s40820-021-00779-0.

[7] R. Mouazer, I. Thijs, S. Mullens, J. Luyten, SiC foams produced by gel casting: synthesis and characterization, Adv. Eng. Mater. 6 (2004) 340–343, https://doi.org/10.1002/adem.200400009.

[8] S. Dong, Y. Katoh, A. Kohyama, Preparation of SiC/SiC composites by hot pressing, using Tyranno-SA fiber as reinforcement, J. Am. Ceram. Soc. 86 (2003) 26–32, https://doi.org/10.1111/j.1151-2916.2003.tb03272.x.

[9] M.Z.E. Becker, N. Shomrat, Y. Tsur, Recent advances in mechanism research and methods for electric-field-assisted sintering of ceramics, Adv. Mater. 30 (2018), 1706369, https://doi.org/10.1002/adma.201706369.

[10] I. Gibson, D. Rosen, B. Stucker, M. Khorasani, Additive Manufacturing Technologies, 17, Springer, New York, 2014, p. 195.

[11] C.A. Chatham, T.E. Long, C.B. Williams, A review of the process physics and material screening methods for polymer powder bed fusion additive manufacturing Progr, Polym. Sci. 93 (2019) 68–95, https://doi.org/10.1016/j.progpolymsci.2019.03.003.

[12] S.F.S. Shirazi, S. Gharehkhani, M. Mehrali, H. Yarmand, H.S.C. Metselaar, N. A. Kadri, N.A.A. Osman, A review on powder-based additive manufacturing for tissue engineering: selective laser sintering and inkjet 3D printing, Sci. Technol. Adv. Mater. 16 (2015), 033502, https://doi.org/10.1088/14686996/16/3/033502.

[13] C. Jiao, J. Gu, Y. Cao, D. Xie, H. Liang, R. Chen, T. Shi, L. Shen, C. Wang, Z. Tian, X. Yi, Preparation of Al_2O_3-ZrO_2 scaffolds with controllable multi-level pores via digital light processing, J. Eur. Ceram. Soc. 40 (2020) 6087–6094, https://doi.org/10.1016/j.jeurceramsoc.2020.06.024.

[14] L. Rueschhoff, W. Costakis, M. Michie, J. Youngblood, R. Trice, Additive manufacturing of dense ceramic parts via direct ink writing of aqueous alumina suspensions, Int. J. Appl. Ceram. Technol. 13 (2016) 821–830, https://doi.org/10.1111/ijac.12557.

[15] L. Yang, S. Tang, G. Li, L. Qian, J. Mei, W. Jiang, Z. Fan, Layered extrusion forming of complex ceramic structures using starch as removable support, Ceram. Int. 45 (2019) 21843–21850, https://doi.org/10.1016/j.ceramint.2019.07.193.

[16] H. Zhang, Y. Yang, B. Liu, Z. Huang, The preparation of SiC-based ceramics by one novel strategy combined 3D printing technology and liquid silicon infiltration process, Ceram. Int. 45 (2019) 10800–10804, https://doi.org/10.1016/j.ceramint.2019.02.154.

[17] M. Yaghtin, A. Yaghtin, Z. Tang, T. Troczynski, Improving the rheological and stability characteristics of highly concentrated aqueous yttria stabilized zirconia slurries, Ceram. Int. 46 (2020) 26991–26999, https://doi.org/10.1016/j.ceramint.2020.07.176.

[18] A. Dolganov, M.T. Bishop, G.Z. Chen, D. Hu, Rheological study and printability investigation of titania inks for Direct Ink Writing process, Ceram. Int. 47 (2021) 12020–12027, https://doi.org/10.1016/j.ceramint.2021.01.045.

[19] Z. Goharibajestani, O. Akhlaghi, C. Akaoglu, F. Afghah, N. Khani, A. Hodaei, B. Koc, O. Akbulut, Incorporating steric hindrance into the additive design enables a robust formulation of alumina ink for extrusion-based 3D printing, ACS. Appl. Polym. Mater. 1 (2019) 3279–3285, https://doi.org/10.1021/acsapm.9b00704.

[20] S. Tang, L. Yang, G. Li, X. Liu, Z. Fan, 3D printing of highly-loaded slurries via layered extrusion forming: parameters optimization and control, Addit. Manuf. 28 (2019) 546–553, https://doi.org/10.1016/j.addma.2019.05.034.

[21] E. Kayacan, B. Ulutas, O. Kaynak, Grey system theory-based models in time series prediction, Expert Syst. Appl. 37 (2010) 1784–1789, https://doi.org/10.1016/j.eswa.2009.07.064.

[22] R. Chen, Y. Li, R. Xiang, S. Li, Effect of particle size of fly ash on the properties of lightweight insulation materials, Construct. Build. Mater. 123 (2016) 120–126, https://doi.org/10.1016/j.conbuildmat.2016.06.140.

[23] J. Liu, R. Wang, F. Gao, J. Zhou, K. Cen, Rheology and thixotropic properties of slurry fuel prepared using municipal wastewater sludge and coal, Chem. Eng. Sci. 76 (2012) 1–8, https://doi.org/10.1016/j.ces.2012.04.010.

[24] S. Baud, F. Thevenot, C. Chatillon, High temperature sintering of SiC with oxide additives: IV. Powder beds and the influence of vaporization on the behaviour of SiC compacts, J. Eur. Ceram. Soc. 23 (2003) 29–36, https://doi.org/10.1016/S0955-2219(02)00070-5.

[25] L. Guo, J. Yang, Y. Feng, T. Qiu, B. Chen, W. Wan, Preparation and properties of AlN ceramic suspension for non-aqueous gel casting, Ceram. Int. 42 (2016) 8066–8071, https://doi.org/10.1016/j.ceramint.2016.02.004.

[26] A.U. Khan, N. Mahmood, P.F. Luckham, Rheological characterization of alumina ceramic suspensions in presence of a dispersant and a binder, J. Dispersion Sci. Technol. 33 (2012) 1210–1217, https://doi.org/10.1080/01932691.2011.605646.
[27] S. Asakura, N. Imai, F. Oosawa, Theory of mechanochemical systems, J. Polym. Sci. 13 (1954) 499–510, https://doi.org/10.1002/pol.1954.120137110.
[28] D. Lao, W. Jia, S. Li, D. Hei, R. Chen, Effect of residual compressive stress on thermal shock resistance and microstructure of Al_2O_3–ZrO_2 reticulated porous ceramics, Mater. Res. Express 6 (2019), 105209, https://doi.org/10.1088/2053-1591/ab4162.
[29] J. Smay, J. Cesarano, J. Lewis, Colloidal inks for directed assembly of 3-D periodic structures, Langmuir 18 (2002) 5429–5437, https://doi.org/10.1021/la0257135.
[30] J. Mewis, N.J. Wagner, Thixotropy. Adv. Colloid. Interfac. 147 (2009) 214–227, https://doi.org/10.1016/j.cis.2008.09.005.
[31] J.C. Baudez, Physical aging and thixotropy in sludge rheology, Appl. Rheol. 18 (2008) 134951–134958, https://doi.org/10.1515/arh-2008-0003.
[32] J. Deng, Grey control system, J. Huazhong Univ. Sci. Technol. 3 (1982) 9–18.
[33] R. Chen, W. Jia, Q. Shan, Y. Ling, D. Lao, Y. Wang, D. Hei, A novel design of Al_2O_3-ZrO_2 reticulated porous ceramics with hierarchical pore structures and excellent properties, J. Eur. Ceram. Soc. 39 (2019) 1877–1886, https://doi.org/10.1016/j.jeurceramsoc.2019.01.007.
[34] M. Li, Y. Li, D. Ouyang, R. Chen, S. Li, The impact of alumina bubble particle size on the microstructure and physical properties of mullite castables, Ceram. Int. 45 (2019) 1928–1939, https://doi.org/10.1016/j.ceramint.2018.10.085.
[35] C. Mair, G. Kadoda, M. Lefley, K. Phalp, C. Schofield, M. Shepperd, S. Webster, An investigation of machine learning based prediction systems, J. Syst. Software 53 (2000) 23–29, https://doi.org/10.1016/S0164-1212(00)00005-4.
[36] J.H. She, K. Ueno, Densification behavior and mechanical properties of pressureless-sintered silicon carbide ceramics with alumina and yttria additions, Mater. Chem. Phys. 59 (1999) 139–142, https://doi.org/10.1016/S0254-0584(99)00039-5.
[37] T. Grande, H. Sommerset, E. Hagen, K. Wiik, M.A. Einarsrud, Effect of weight loss on liquid-phase-sintered silicon carbide, J. Am. Ceram. Soc. 80 (1997) 1047–1052, https://doi.org/10.1111/j.1151-2916.1997.tb02945.x.